Research Square

Preprints are preliminary reports that have not undergone peer review.
They should not be considered conclusive, used to inform clinical practice,
or referenced by the media as validated information.

Interior spacetime curvature and positron yield of a stationary capsule enclosed by a chopped near-light-speed energy shell

Hasan Börekci

hborekci@hotmail.com.tr

HB ZECHMANN Medical Company

Article

Keywords: Börekci metric, energy shell, electron storage, truncated photon, dynamical Casimir effect, time dilation, positron production, optical clocks

Posted Date: September 9th, 2026

DOI: https://doi.org/10.21203/rs.3.rs-10960758/v1

License: This work is licensed under a Creative Commons Attribution 4.0 International License.
Read Full License

Additional Declarations: Competing interest reported. The author declares the following competing interest: a patent application for the "Börekci Energy Field — spacetime dilation and antimatter production system" (TÜRKPATENT application no. 2026/011037, 4 July 2026) has been filed by the author. The author declares no other competing interests.

Interior spacetime curvature and positron yield of a stationary capsule enclosed by a chopped near-light-speed energy shell

Hasan Börekci

R&D Director, HB ZECHMANN Medical Company, Manisa Teknokent, Manisa, Türkiye; independent researcher not employed by any state-affiliated institution

Correspondence: hborekci@hotmail.com.tr — ORCID 0000-0001-9137-6342 — Scopus Author ID 55903343000

Declaration. Dr. Hasan Börekci received no institutional support for the design or writing of this article or of the apparatus and is not employed by any state-affiliated institution; the work was carried out entirely with the author's own means. The conception, planning and apparatus design are the author's own. Artificial intelligence was used for the literature search, the calculations and the page layout. A patent application for the "Börekci Energy Field — spacetime dilation and antimatter production system" has been filed with TÜRKPATENT (no. 2026/011037, 4 July 2026).

Abstract

We ask how strongly the spacetime inside a stationary capsule is curved when the capsule is enclosed, pole to pole, by a stored near-light-speed electron–laser energy shell that is cut for one second every five minutes, and how the chopping affects positron production. The revised triple-capsule apparatus stores $\gamma = 59.7$ electrons in a 5 T superconducting guide layer ($\tau \approx 0.11$ s, ≈140 kJ) and adds a 20 kJ superconducting-RF photon shell. Three epistemic layers are kept apart: standard general relativity (L2), the author's conviction that the interior Lorentz factor equals that of the shell electrons (L1), and a one-parameter test metric (L3). In L2 the shell term at the cavity centre is $\Phi_s/c^2 = -3.7\times10^{-40}$ (1.7×10^{7} times the previous design), the chopper converts it into a 3.33 mHz square wave without bending the interior field (extra curvature $\leq 3\times10^{-54}$ m^{-2}), and lock-in detection tightens the laboratory bound on the coupling parameter 10^{7}-fold, to $\xi < 1.4\times10^{21}$. The chopper reduces positron output by only 0.3% while delivering 288 time-stamped bursts per day that measure the stored shell energy. The 24-hour yield is $3.2–6.5\times10^{20}$ fast positrons, $0.6–1.3\times10^{18}$ trappable; no other antimatter species is produced.

Keywords: *Börekci metric; energy shell; electron storage; truncated photon; dynamical Casimir effect; time dilation; positron production; optical clocks*

Introduction

General relativity predicts, with a century of confirmed precision, how a mass or an energy flow curves spacetime. The configuration studied here is nevertheless unusual: a stationary, thick-walled inner capsule is enclosed pole to pole by an electron flow at very nearly the speed of light ($\beta = 0.99986$) together with a laser ring; the electrons are stored for a tenth of a second in a superconducting guide field so that the shell becomes an energy layer rather than a passing current; the shell is wrapped by a second electron shell, by 20 T toroidal magnets and by a rotating platform; and every five minutes the whole shell is cut for one second. The question is twofold. Does the spacetime inside the inner capsule differ measurably from the spacetime outside — and what does the periodic cutting of the shell do to that difference? And what quantity and species of antimatter does the apparatus produce, and how does the cutting change it?

The author's conviction (layer L1) is a symmetry argument drawn from the principle of relativity: enclosing a stationary body with a near-light-speed energy shell should be "equivalent" to the body moving at that speed, so that the interior time-dilation factor equals the Lorentz factor of the shell electrons, $\Gamma_{in} = \gamma_e \approx 60$. Standard general relativity (layer L2) does not accept the argument: the shell

acts on the cavity only through its energy–momentum tensor, and the resulting potential is of order 10^{-40}. Rather than choosing between the two views, this article keeps them on the same page and reduces their difference to one measurable parameter, ξ, in a test metric (layer L3, Methods). Every result below is therefore stated three times — L2, L1 and L3 — and the "dual-framing rule" ($\xi = 1$ standard relativity; $\xi \gg 1$ the hypothesis) is never mixed.

Two developments motivate this revision of the author's earlier design [1, 2]. First, a design audit found that the shell of the earlier apparatus carried only 11 mJ at any instant, because the electrons crossed the capsule in 63 ns and stopped in the anode: what acts on spacetime is energy in flight, not power. The revised design (BEF-2026-R) therefore stores the shell electrons magnetically and adds a superconducting-RF (SRF) photon shell, raising the enclosed near-light-speed energy to 158 kJ. Second, Rukan, Gulla and Skaar [3] showed that a single photon cut by a fast shutter becomes, globally, a mixture of 0, 1, 2, … photons created from the vacuum (a form of the dynamical Casimir effect [4, 5]) while remaining locally indistinguishable from the original photon on one side of the cut and from the vacuum on the other. The five-minute chopper of the apparatus is the direct macroscopic analogue of that experiment, and the question of whether the cut bends the field inside the shell is answered here with the same quantum-field-theoretical tools.

The significance of the work lies in three points. It gives the first quantitative energy–momentum budget for a stored, chopped, enclosing energy shell and shows what the chopper does — and does not do — to the interior spacetime and to the antimatter yield. It shows that the chopper, although it cannot bend the interior field in standard relativity, is what makes the shell contribution measurable by lock-in detection, and tightens the laboratory bound on the metric coupling of confined dynamic energy by seven orders of magnitude. And it defines an experiment that can falsify or confirm the L1 claim decisively with a chip-scale atomic clock, while producing a positron flux 10^4 times that of the strongest existing slow-positron source [6].

Results

The revised apparatus

The apparatus (Figures 1–3, Table 1; full description in Methods) consists of three nested capsules on a common vertical axis in a sealed rock cavern. The inner capsule is a 12 m × 10 m prolate ellipsoid with a four-layer wall (SiC-SiC, tungsten–steel, lead, water) enclosing a 43.9 m³ cavity at 1 atm that holds the test subject, a clock and a camera. On its outer surface a 50 cm REBCO superconducting layer produces a 5 T field tangent to the surface; together with 10 T pole magnets it forms a magnetic mirror (5 T at the equator, 10 T at the polar throats). A 30 MV / 20 mA electron arc between tungsten–rhenium electrodes at the poles injects $\gamma = 59.7$ electrons into this field, where synchrotron radiation limits their confinement to $\tau \approx 0.11$ s; the steady-state stored energy is 140 kJ in a 4 cm layer of 2.8×10^{16} electrons, one thousandth of the Brillouin density limit [7]. A 20 kW, 1064 nm laser ring runs parallel to the electrons, and a niobium SRF cavity wall (1.3 GHz, $Q = 10^{10}$ [8]) one metre outside the coil layer stores 20 kJ of electromagnetic energy as a "photon shell". A second 30 MV / 20 mA arc runs in the 3.1 m gap between the outer sphere (16 m inner diameter) and the extra outer sphere (28 m inner diameter); two 20 T REBCO toroidal rings [9] and a base platform rotating at 120 rpm complete the structure. The chopper cuts all three channels — laser (Pockels cell, 1 ns edge), arc (cathode grid, 1 µs edge) and SRF (active dump coupler) — for $\tau_c = 1$ s every $T_c = 300$ s (Figure 5a); the cut is long enough for the stored shell (0.11 s) and the SRF shell (1.2 s decay time) to empty, so that the modulation depth is 99.98%. The anodes are thick converters followed by a solid-neon moderator and a multicell Surko trap line [10, 11].

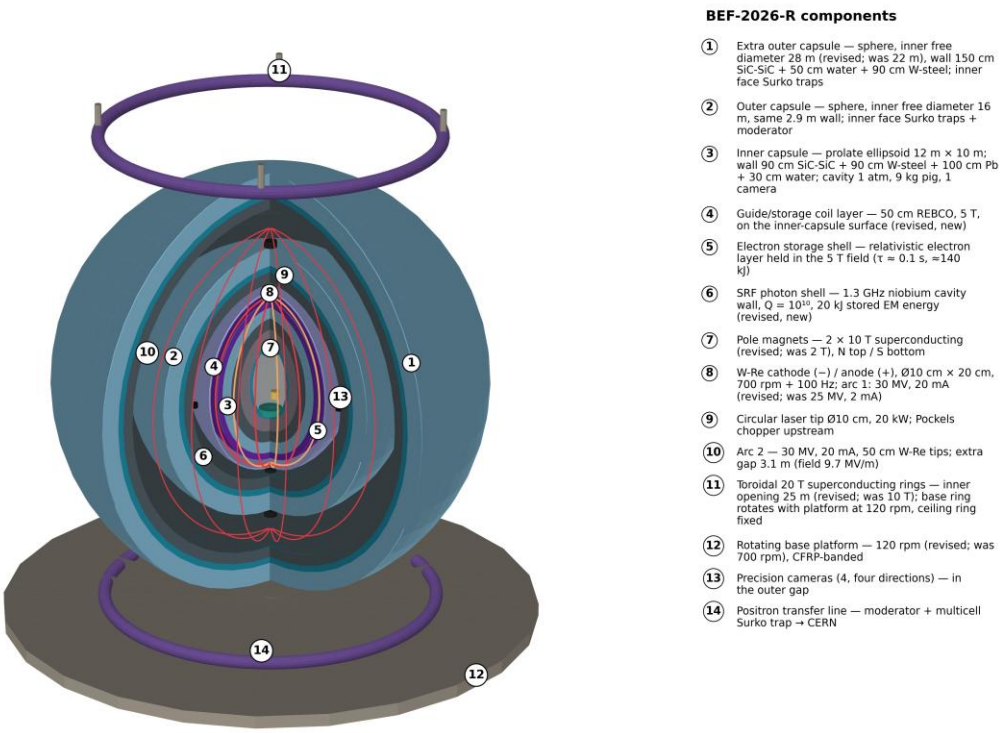


Figure 1. Three-dimensional isometric cutaway of BEF-2026-R (legend in Figure legends).

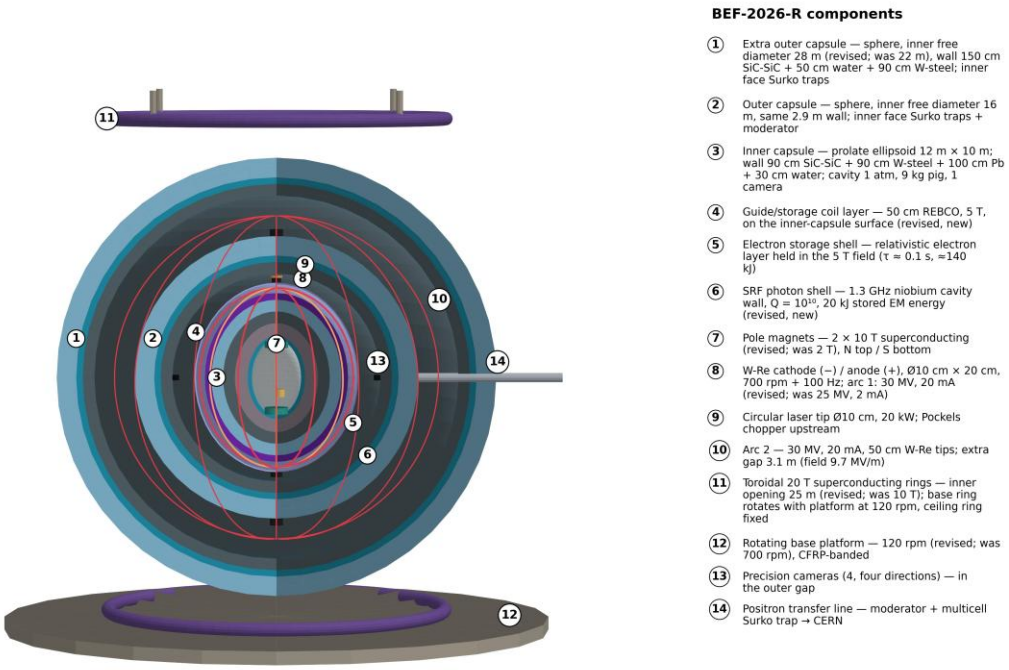


Figure 2. Side view, vertical section (legend in Figure legends).

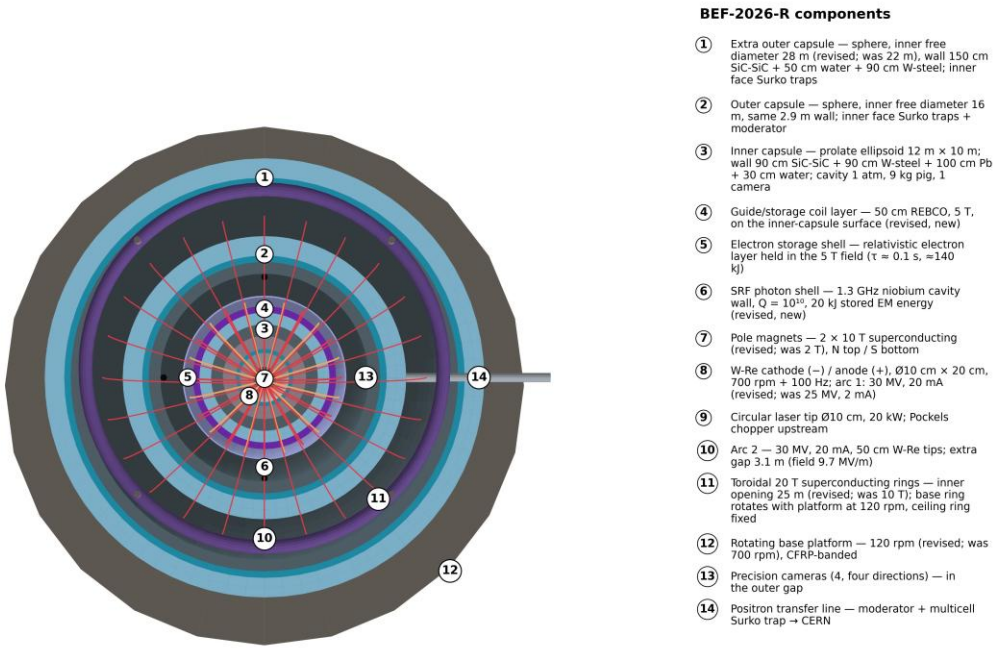


Figure 3. Top view, equatorial section (legend in Figure legends).

Table 1. BEF-2026-R apparatus parameters (changed items marked *).

Component	Value
Site	Sealed rock cavern under a large mountain
Extra outer capsule *	Sphere, inner free diameter 28 m (outer 33.8 m), 0 atm; wall 150 cm SiC-SiC + 50 cm water + 90 cm tungsten–steel; inner face Surko traps; mass 43 070 t
Outer capsule	Sphere, inner free diameter 16 m (outer 21.8 m), 0 atm; same wall; inner face solid-neon moderator + Surko traps; mass 15 480 t; 4 cameras in the gap
Inner capsule	Prolate ellipsoid 12 m × 10 m; wall 90 cm SiC-SiC + 90 cm tungsten–steel + 100 cm Pb + 30 cm water; cavity 43.9 m³ at 1 atm; mass 4 200 t
Guide/storage coil layer *	50 cm REBCO on the inner-capsule surface, 5 T tangential; mass 1 070 t; 1.8 GJ
Pole magnets *	2 × 10 T superconducting (N top, S bottom)
Electron arc 1 *	30 MV, 20 mA (600 kW), $\gamma = 59.7$; W-Re electrodes Ø10 cm, 700 rpm + 100 Hz
Electron storage shell *	Mirror-confined, $\tau \approx 0.11$ s, ≈140 kJ, 2.8×10^{16} electrons, ~4 cm layer
Laser	Ø10 cm ring, 20 kW CW, 1064 nm; Pockels chopper
SRF photon shell *	Niobium wall, 1.3 GHz, $Q = 10^{10}$, 20 kJ stored; 16 kW at 2 K
Electron arc 2 *	30 MV, 20 mA in the 3.1 m extra gap (9.7 MV/m)
Toroidal rings *	2 × 20 T REBCO, inner opening 25 m, 10.2 GJ each; 0.98 T at the centre
Base platform *	120 rpm; rim speed 212 m/s; CFRP-banded
Chopper *	1 s cut every 300 s: Pockels cell (1 ns) + cathode grid (1 µs) + SRF dump coupler; 288 cycles, 576 switchings per day
Positron line *	W-Re converter → solid-neon moderator (~10^{-2}) → multicell Surko trap (~20%) → transfer line

Metric potential at the cavity centre

In the linearized Einstein equations every source contributes $\Phi/c^2 = -G\,M_{eff}/(c^2\,r)$ at the cavity centre, with $M_{eff} = M$ for rest mass, E/c^2 for field energy and $2E/c^2$ for energy moving at the speed of light or stored as relativistic kinetic energy (the pressure terms of the energy–momentum tensor double the source). Table 2 lists every source. The wall masses dominate, $\Phi/c^2 = -4.27\times10^{-21}$, a slowing of 369 attoseconds per day that is only 1.8 times below the fractional difference resolved by Bothwell et al. [12] with a 90-hour average; it is static and cancels in the ON/OFF difference. What survives the difference is the rotation (-3.3×10^{-34}), the magnetic and electrostatic fields (-1.0×10^{-35}) and the shell itself, $\Phi_s/c^2 = -3.7\times10^{-40}$, of which the stored electron layer contributes -3.2×10^{-40} and the SRF photon shell -4.4×10^{-41}. Storage raises the shell term 1.7×10^{7}-fold over the previous design (-2.2×10^{-47}). Its meaning must be stated plainly: in standard relativity the shell term is still 10^{21} times below the resolution of the best clocks; the gain lies in the bound that can be placed on the hypothesis, not in direct measurability. The curvature scale of the 158 kJ spread over the 1 516 m³ gap is $K = 8\pi G\,u/c^4 = 2.2\times10^{-41}$ m^{-2} (inside the stored layer, 2.0×10^{-39} m^{-2}), against $\sim10^{-23}$ m^{-2} at the Earth's surface.

Table 2. Contributions to the metric potential at the cavity centre (L2, ξ = 1); v1 is the previous design.

Source	Effective energy / mass	Distance	Φ/c² (BEF-2026-R)	Φ/c² (v1)	In the ON/OFF difference
Inner-capsule wall + coil layer	5 270 t	4.0 m	-9.8×10^{-22}	-7.8×10^{-22}	cancels (static)
Outer-capsule wall	15 480 t	9.45 m	-1.22×10^{-21}	-1.22×10^{-21}	cancels
Extra-capsule wall	43 070 t	15.45 m	-2.07×10^{-21}	-1.64×10^{-21}	cancels
Walls total	—	—	-4.27×10^{-21} (369 as/day)	-3.64×10^{-21}	cancels
Platform rotation (120 rpm)	0.67 TJ	16.9 m	-3.3×10^{-34}	-5.9×10^{-33}	remains
Toroidal rings (2 × 10.2 GJ)	20.4 GJ	22.1 m	-7.6×10^{-36}	-2.1×10^{-36}	remains
Guide/storage coil layer	1.8 GJ	6.25 m	-2.3×10^{-36}	—	remains
Pole magnets	80 MJ	3.0 m	-2.2×10^{-37}	-8.8×10^{-39}	remains
Electrostatic energy	2.5 MJ	8.0 m	-2.5×10^{-39}	-6.2×10^{-38}	remains
Fields total	—	—	-1.0×10^{-35}	-2.2×10^{-36}	8.8×10^{-31} s/day
Shell 1 transit + laser	2 × 42 mJ	7.0 m	-1.0×10^{-46}	-1.1×10^{-47}	chopper-modulated
Shell 2 transit	2 × 78 mJ	12.45 m	-1.0×10^{-46}	-1.0×10^{-47}	chopper-modulated
Stored electron shell (τ = 0.11 s)	2 × 140 kJ	7.0 m	-3.2×10^{-40}	—	chopper-modulated
SRF photon shell (Q = 10^{10})	2 × 20 kJ	7.5 m	-4.4×10^{-41}	—	chopper-modulated
Near-light-speed shell total Φ_s/c^2	158 kJ	—	-3.7×10^{-40} (3.2×10^{-35} s/day)	-2.2×10^{-47}	1.7×10^{7}-fold
Accumulated heat (24 h, if not removed)	105 GJ	9.0 m	-9.7×10^{-35}	-1.0×10^{-35}	grows linearly

The electron–laser chopper and the spacetime inside the inner capsule

The chopper is the element of the design that most directly addresses the author's question, and its effect must be given in all three layers.

In L2 the analysis follows the truncated-photon result [3]. When the shell is cut, three things happen to the field. (i) Photons are created from the vacuum at the switching edge. For the Pockels cell (transmission 10^{-4} at 1064 nm, $\kappa_0 = 1.13\times10^{-13}$ s; 1 ns edge) the Rukan–Gulla–Skaar bound $\langle n\rangle \le \kappa_0/4T$

+ $\kappa_0^2/16T^2$ gives 2.8×10^{-5} photons per one-dimensional channel; the Ø10 cm beam contains $A/\lambda^2 = 6.9\times10^9$ transverse modes, so each switching creates $N_{DCE} \approx 2.0\times10^5$ photons carrying 3.7×10^{-14} J (Figure 5b) — 3×10^{-11} of the 7.3×10^{15} laser photons in flight. For the electron field the corresponding time scale is $\hbar/2m_ec^2 = 6.4\times10^{-22}$ s, fifteen orders of magnitude shorter than the 1 µs grid edge, so no electron–positron pairs are created from the vacuum by the cut; in the microwave SRF channel the yield is $\sim10^{-11}$ photons per switching. (ii) The extra energy is confined to a transition region of width cT = 30 cm that moves with the light cone; its curvature is 3.2×10^{-54} m^{-2} and its contribution to the cavity potential 9×10^{-59} (with the pressure term). (iii) By the local-equivalence theorem, every local measurement on the shell side of the transition region gives the statistics of the uncut shell and every measurement on the other side gives the statistics of the vacuum: the field inside the shell is locally unchanged by the cut. What the cut does change is the shell's own energy: the 158 kJ layer empties with a 0.11 s time constant and refills in 0.11 s, so that the cavity potential becomes a square wave of amplitude 3.7×10^{-40}, period 300 s and 0.11 s edges (Figure 5a). The metric transient at each edge is $h \approx 2\times10^{-53}$ and the quadrupole radiation 4×10^{-74} W (Supplementary Table S3). The L2 answer is therefore unambiguous: the chopper does not bend the field inside the shell; it turns a static shell term into an alternating one.

That conversion is the chopper's real value. A static potential of 10^{-40} is hidden under the 10^{-21} wall term and under clock drift; an alternating term at 3.33 mHz can be extracted by lock-in detection against the chopper timer. For a clock pair of fractional stability σ_y the exclusion bound on the coupling parameter is $\xi_{excl} = \sigma_y/|\Phi_s/c^2|$; an optical lattice clock reaching 5×10^{-19} after the 288 lock-in cycles of one session excludes $\xi > 1.4\times10^{21}$, against 2.3×10^{28} for the previous design (Figure 6b). Because the required ξ_{L1} and the excludable ξ both scale as $1/\Phi_s$, the 18 orders of magnitude between them do not change; what changes is the absolute bound on the metric coupling of confined dynamic energy, which the revision tightens 10^7-fold.

In L1 the chopper produces a signature that no other element of the design produces. In the test metric the chopper function s(t) multiplies the term $\xi\Phi_s$; with $\xi = \xi_{L1}$ the interior Lorentz factor is $\Gamma_{in} = 59.7$ while the shell is full and 1 during the cut. If the conviction is right, the interior clock runs at the exterior rate for one second every five minutes and then slows 60-fold again: 288 steps per day in the interior clock rate, each of 1 s, phase-locked to the chopper. A chip-scale atomic clock in the cavity would see a 23.6-hour difference after 24 hours; the step structure would distinguish the shell from any static cause. In L3 the ξ-multiplied contribution of the photons created by the cut is $\xi_{L1} \times 9\times10^{-59} \approx 10^{-19}$ and is unmeasurable even under the hypothesis. The three-layer answer to the author's question is thus: L2 — the cut does not bend the interior field ($\leq 3\times10^{-54}$ m^{-2}); L1 — the cut changes the interior rate of time 60-fold every five minutes; L3 — the chopper is what makes the two predictions distinguishable in a single measurement, and with the revision the bound descends to $\xi \sim 10^{21}$.

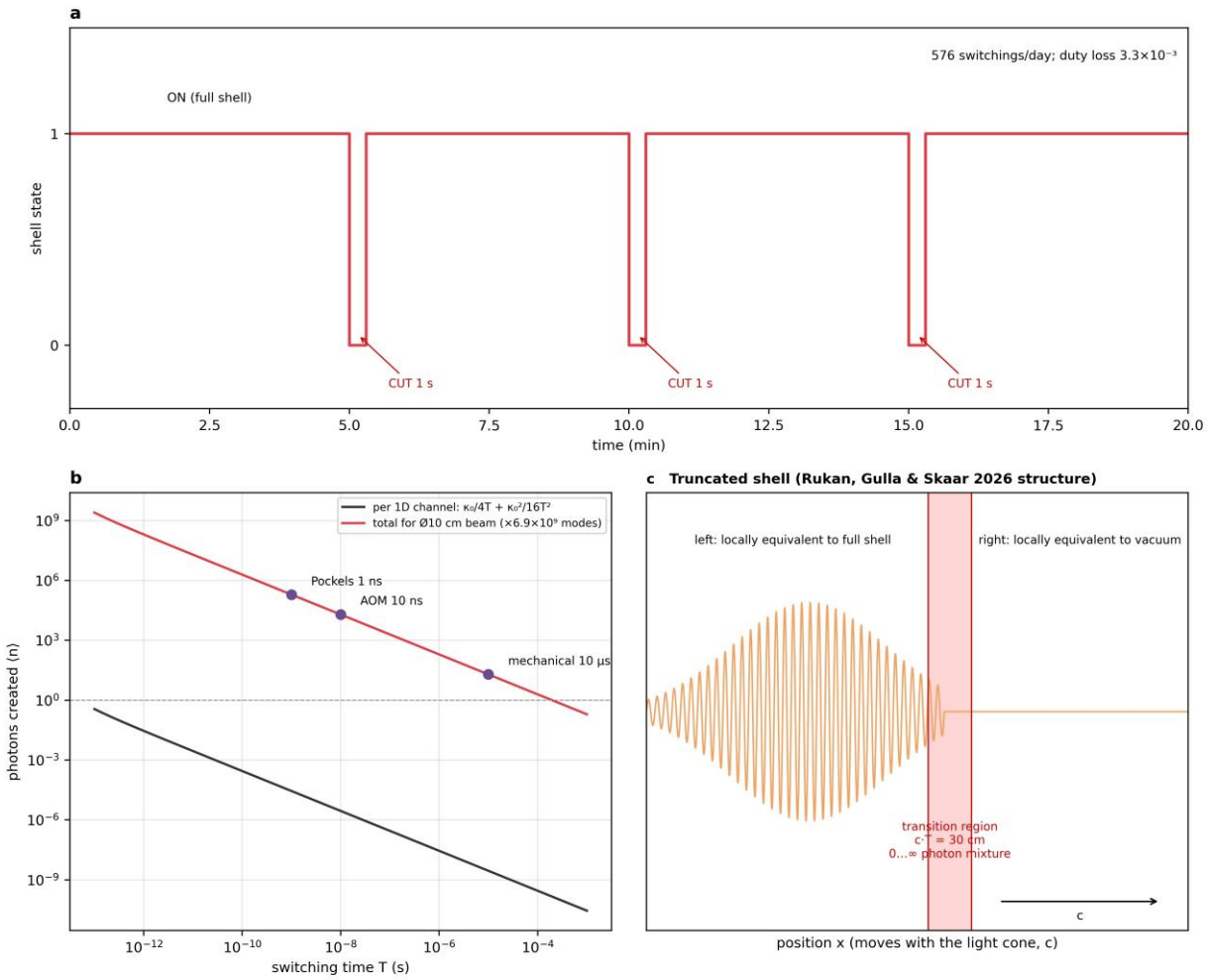


Figure 5. Chopper analysis: a, 5-minute cycle; b, photons created per switching; c, local-equivalence structure (legend in Figure legends).

The chopper and antimatter production

The chopper acts on the positron yield in three ways, and all three are small. First, the duty loss: the arcs are off for 1 s in 300 s, so the electron flux to the anodes and the positron production fall by τ_c/T_c = 0.33% (from 3.24×10^{20} to 3.23×10^{20} fast positrons per day in the conservative case). Second, the burst: at the moment of the cut the stored layer of 2.8×10^{16} electrons descends to the anodes within ~0.1 s, producing 4–8×10^{14} positrons in a single pulse; the instantaneous rate during the burst (4–8×10^{15} s^{-1}) is equal to the steady-state rate, because the stored shell is simply the steady flow accumulated over one confinement time. The burst adds nothing to the daily total, but it is time-stamped: 288 bursts per day, each proportional to the stored charge, give a direct measurement of the shell energy E_{shell} (and hence of Φ_s) to better than 1% in every cycle — the calibration that the L3 analysis requires. Third, the vacuum: the 2×10^5 photons created from the vacuum at each switching have energy 1.17 eV, six orders of magnitude below the pair-creation threshold of 1.022 MeV, and the electron field is not excited at all; the chopper creates no antimatter from the vacuum. The species produced is definite: at 30 MeV the antiproton (5.6 GeV) and muon-pair (211 MeV) thresholds are far out of reach; only positrons are produced, in the anodes, by bremsstrahlung and Bethe–Heitler conversion [13, 14].

The interior Lorentz factor in three layers

Both arcs run at 30 MV, so $\gamma_e = 1 + 30/0.511 = 59.71$ is common to the two shells. In L1, $\Gamma_{in} = 59.71$: while 24 hours pass outside, 24.1 minutes pass in the inner capsule (60.3 interior seconds per exterior hour). In the test metric this requires $\xi_{L1} = (1 - 1/\gamma_e^2)\, c^2/2|\Phi_s| = 1.4\times10^{39}$ (previously 2.3×10^{46}). In L2, $\Gamma_{in} - 1 = 3.7\times10^{-40}$, i.e. 3.2×10^{-35} s per day. In L3 the exclusion bounds are 2.7×10^{27} for a chip-scale clock ($\sigma_y \sim 10^{-12}$), 2.7×10^{24} for a hydrogen maser (10^{-15}), 2.7×10^{21} for an optical lattice clock (10^{-18}) and 1.4×10^{21} with chopper lock-in (Figure 6b; Supplementary Table S4). If L1 is right, the cheapest clock in the cavity sees the effect; if it is wrong, the same measurement sets the tightest laboratory bound to date on the metric coupling of confined dynamic energy.

Antimatter yield of a 24-hour session

The two arcs deliver 2.16×10^{22} electrons to the tungsten–rhenium anodes in 24 hours. With a total fast-positron yield of $1.5–3.0\times10^{-2}$ per 30 MeV electron [13, 14], the session produces $3.2–6.5\times10^{20}$ fast positrons (295–589 ng; $3.7–7.5\times10^{15}$ s^{-1}), fifteen times the previous design. Fast MeV positrons cannot be trapped directly: the solid-neon moderator converts ~1% into eV positrons ($3.7–7.5\times10^{13}$ s^{-1}, 4×10^{4} times the NEPOMUC source [6]) and the multicell Surko trap accumulates ~20% of those, $0.6–1.3\times10^{18}$ per day (0.6–1.2 ng), three hundred times the previous design (Figure 6c; Supplementary Table S5). The honest limit is the trap: the largest positron numbers accumulated so far are $\sim10^{10}$, and the multicell proposal targets 10^{12} [11]; the production, not the accumulation, is what the apparatus changes. Annihilation of untrapped positrons produces $3.2–6.5\times10^{20}$ polarization-entangled 511 keV photon pairs per day, none of which cross the 100 cm lead wall (transmission 10^{-74}); the only quantum link between the cavity and the outside remains the gravitational field itself.

Gains of the revision

Figure 6 compares the stated design with the revised design. Raising the near-light-speed energy surrounding the inner capsule from 11 mJ to 158 kJ raises the shell term 1.7×10^{7}-fold, the field terms 4.6-fold and the wall term by 17%; the ξ bound tightens 10^{7}-fold; fast-positron production rises 15-fold and the number of trappable positrons 300-fold; three design contradictions (a 10 cm gap with a 300 MV/m field, 700 rpm for a 33.8 m structure, walls incompatible with the stated masses) are removed, the spin-up energy falls 15-fold (2 770 → 187 MWh) and the continuous power rises 3-fold (6.4 → 20.2 MW). The structure of the three-layer answer does not change (Supplementary Tables S1, S6).

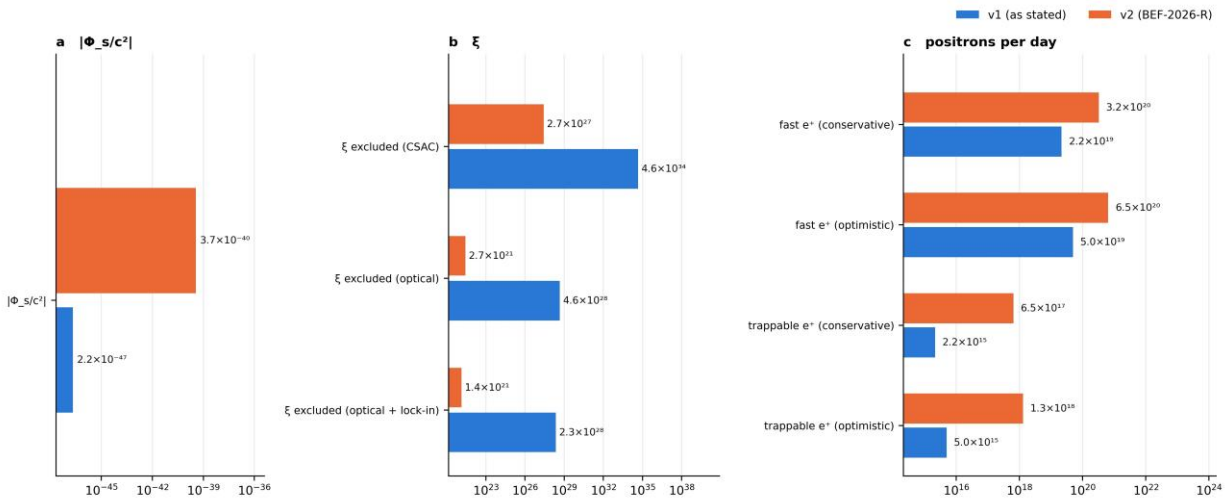


Figure 6. Stated (v1) versus revised (BEF-2026-R) design: a, shell term; b, ξ bounds; c, positrons per day (legend in Figure legends).

Discussion

Standard relativity and the author's conviction

The author's physical intuitions rest on four ideas: that a near-light-speed energy layer surrounding a stationary body is equivalent, by the principle of relativity, to the body moving at that speed; that the energy density of the shell, not its total energy, is what matters, so that a thin layer around a small volume is the right geometry; that rapid change of the energy distribution (rotation, vibration, chopping) is a source in its own right; and that the shell separates the interior quantum field from the exterior one. Standard relativity answers each point without ambiguity. The equivalence argument fails because the interior metric is fixed by the energy–momentum tensor integrated over the shell, not by the velocity of its constituents: a shell of electrons at $\gamma = 60$ and a shell of the same energy at rest curve the interior identically (Birkhoff's theorem [15] and Israel's junction conditions [16]); the gravitational field of light and of particle beams has been computed exactly [17–21] and is of the order found here. The density argument is correct in direction (design principle 1 is strengthened 10^{7}-fold by storage) but the shell remains 10^{14} times below the rest-energy density of the enclosed body. Rapid change radiates gravitational waves at the 10^{-32} W level for the rotation and 10^{-74} W for the chopper, with cavity transients of 10^{-36} and 10^{-53} (Supplementary Table S3); the gravitomagnetic frame-dragging of the rotating 45 000 t structure is 3.3×10^{-20} rad/s, 10^{5} below Gravity Probe B [22]. And the shell does not separate quantum fields: 100 cm of lead separates photons, not the metric, and the field inside the shell is locally identical to the field outside (local equivalence [3]).

The three-layer framework is the article's answer to this disagreement. The author's conviction is not treated as a result but as the parameter $\xi_L1 = 1.4\times10^{39}$ of a test metric; today's clocks exclude $\xi > 2.7\times10^{21}$, and the chopper lock-in reaches 1.4×10^{21}. Eighteen orders of magnitude remain open, and the apparatus can close them in a single session in either direction.

Could the chopper-induced changes in spacetime and the quantum field enhance the curvature? — the author's interpretation

The author holds that the chopper is more than a modulator, and this section states that position together with the bounds that standard theory places on it, so that the reader can see exactly where the two part company. Three mechanisms are put forward.

The first is non-adiabatic switching as a source. In L2 the cut excites the metric only through the changing energy–momentum of the emptying shell — a transient $h \approx 2\times10^{-53}$ at each edge that radiates away — and the interior returns to its static value within the 0.11 s emptying time. In the author's reading the interior spacetime may possess a finite temporal response, in the sense of the temporal-response framework of Lemeshko [23] (a lapse function that relaxes towards its source with a response coefficient), so that a periodic drive at the chopper frequency could pump the interior lapse rather than let it relax: 288 identical kicks per day, all phase-locked. If such a response time existed, the effect would depend on the chopper period, and the coupling would be frequency-dependent, $\xi = \xi(\omega)$. This is a hypothesis of layer L3, and it is testable: the measurement protocol scans the period T_c over 300 s, 60 s and 10 s and compares the lock-in amplitudes; in L2 all three amplitudes are equal (3.7×10^{-40}) and a period-dependent amplitude would be the signature of the effect.

The second is the quantum state of the cut field. The truncated-photon analysis shows that the global state after the cut is (one forward + one backward excitation) × (multimode squeezed vacuum). Squeezed states of the electromagnetic field are the textbook example of a state with regions of negative energy density; in semiclassical gravity a negative energy density sources curvature of the opposite sign, so that the alternating positive and negative regions of the squeezed vacuum in the transition layer curve

spacetime in alternating directions. The author's reading is that a coherent, repeated preparation of such states around the inner capsule could add to the curvature of the interior. Standard theory bounds the magnitude: quantum inequalities [24] limit the time-averaged negative energy density to about $\hbar c/(cT)^4 \sim 10^{-24}$ J m^{-3} for a 1 ns edge, i.e. a curvature of order 10^{-66} m^{-2}, twelve orders below that of the cut's own DCE energy; translated into a cavity potential it is $\sim 10^{-71}$, thirty orders below the shell term, and multiplied by ξ_L1 it is still $\sim 10^{-32}$. The mechanism exists, its sign alternates, and its L2 magnitude is negligible.

The third is coherence and reset. The author's conviction attributes the interior time dilation not to the energy of the shell but to its coherent, near-light-speed motion as a whole. On that reading a shell that runs uninterrupted may "saturate" — its interior effect may reach a steady value — whereas a shell that is periodically emptied and rebuilt re-establishes its coherent state 288 times a day; the author expects the rebuilt state to couple to the interior at least as strongly as the continuous one and possibly more strongly, in the way that a pulsed drive transfers more energy to a resonant system than a continuous one of the same average power. In standard relativity there is no such coherence coupling — the interior sees only the energy–momentum tensor — and the expectation cannot be quantified within L2; it belongs to L1. The author's position, stated plainly, is that the chopper's changes to the spacetime and to the quantum field around the inner capsule are more likely to increase than to decrease the interior curvature, that the positive effect, if it exists, will appear as a chopper-period-dependent clock signal, and that the protocol of this article measures exactly that signal. The bounds given above are what standard theory says; the measurement is what will decide.

Literature for and against

The literature since 2019 supports the experimental programme on several points and contradicts the L1 claim on others (Supplementary Note S7). In favour: gravitational redshift is now resolved across a millimetre [12]; the gravitational coupling of milligram and millimetre masses has been measured [25, 26]; analogue horizons in Bose–Einstein condensates and in optical fibres exhibit Hawking radiation [27–29]; the dynamical Casimir effect has been observed [5] and the truncated photon computed [3]; laser-driven positron beams and pair plasmas exist [13, 14, 30]; 20 T REBCO coils have been demonstrated [9]; and the ultra-high-energy neutrino KM3-230213A [31] shows that Lorentz invariance holds to 10^{20} eV, which is at once a support for the tools used here and a constraint on any hypothesis that would modify the metric coupling. Against: the equivalence-principle test of MICROSCOPE [32] and the gravitational-wave tests of general relativity [33] leave no room for a velocity-dependent coupling of the size L1 requires; the claimed gravitational shielding by superconductors [34] was never reproduced; and the shielding theorems of Le Floch and LeFloch [35] show that the Einstein constraints can be localized only at the price of exotic matter, which the shell does not contain. The author's collective answer is the three-layer framework: none of these results measures the metric coupling of a confined, stored, chopped near-light-speed energy layer directly, and the bound of this article, $\xi < 1.4\times10^{21}$, would be the first.

Limitations and the pre-experiment

The calculations are linearized and use idealized geometry; the confinement time is set by synchrotron cooling alone and neglects instabilities, which at 10^{-3} of the Brillouin limit are not expected to dominate; the positron yields are interpolated from 25–35 MeV converter data; the SRF energy of 20 kJ is near the engineering limit set by the 2 K heat load; and the cost figures are order-of-magnitude. The capital cost (3–15 billion dollars) and the animal subject are the two points on which the design will be judged most severely, and the author accepts both criticisms; ethics-committee approval is a precondition of any live-animal work, and a mannequin with clocks is the natural first subject. A small-scale pre-experiment is

defined in Methods: a table-top stored-electron layer around a clock, chopped at 1 Hz, with a two-channel (optical and microwave) lock-in, which tests the whole measurement chain and sets a first bound on ξ at the 10^{30} level before any large investment is made.

Methods

Three-layer framework and the test metric

The three layers are: L2, standard general relativity in the linearized weak-field approximation; L1, the author's conviction Γ_in = γ_e; L3, a one-parameter test metric (the Börekci metric) that contains both as limits,

$$ds^2 = -(1 + 2\Phi_B/c^2)\, c^2 dt^2 - (4/c)(A_B \cdot dx)\, c\, dt + (1 - 2\Phi_B/c^2)(dx^2 + dy^2 + dz^2) \quad (1)$$

$$\Phi_B(x, t) = \Phi_0(x) + \xi \cdot s(t) \cdot \Phi_s(x) + \Phi_acc(t), \quad A_B = A_0 + \xi \cdot s(t) \cdot A_s \quad (2)$$

where Φ_0 and A_0 are the potentials of the static masses and fields, Φ_s and A_s those of the near-light-speed shell (transit, stored electrons, laser and SRF energy), $s(t) \in \{0, 1\}$ the chopper function and Φ_acc the potential of accumulated heat, which is not multiplied by ξ. The shell potential at the cavity centre is

$$\Phi_s(x) = -(G/c^2) \int [T^{00} + T\text{^}xx + T\text{^}yy + T\text{^}zz]_shell(x') / |x - x'|\, d^3x' \approx -2G\, E_shell /(c^2\, r_eff) \quad (3)$$

and the interior clock rate and Lorentz factor are

$$d\tau_in/dt = \sqrt{(1 + 2\Phi_B/c^2)}, \quad \Gamma_in(t) = dt/d\tau_in = [1 + 2\Phi_B(t)/c^2]\text{^}(-1/2) \quad (4)$$

so that ξ = 1 reproduces standard relativity and the L1 statement Γ_in = γ_e fixes

$$\xi_L1 = (1 - 1/\gamma_e^2) \cdot c^2 / (2\, |\Phi_s|) \quad (5)$$

The measured quantity is the ON/OFF difference of the logarithmic clock ratio, S = Δ ln(N_in/N_out)|_(ON−OFF) = ξ Φ_s/c² for small Φ, extracted by lock-in at the chopper frequency; the exclusion bound is ξ_excl = σ_y/|Φ_s/c²|. Birkhoff's theorem [15] and the Israel junction conditions [16] fix the L2 limit; the temporal-response framework of Lemeshko [23] is the closest published language for a frequency-dependent ξ.

Apparatus

The experiment is installed in a sealed rock cavern under a large mountain. The architecture consists of three nested capsules on a common vertical axis, a stored energy shell wrapping the inner capsule, a second electron shell in the extra gap, two toroidal rings and a rotating base platform (Figures 1–3, Table 1). The author's original values and the reason for every change are given in Supplementary Table S1.

Inner capsule, cavity and coil layer

The inner capsule is a prolate ellipsoid with semi-axes a = 6 m and b = 5 m; the 3.1 m four-layer wall leaves a cavity of a = 2.9 m and b = 1.9 m (43.9 m³). The 90 cm SiC-SiC is the electrical and optical isolation, the 90 cm tungsten–steel and 100 cm lead the gamma and bremsstrahlung shield (transmission 10^{-74} at 511 keV), the 30 cm water the circulating cooling. The cavity holds air at 1 atm, a 9 kg pig in a protective suit and one camera; the round-pole 10 T superconducting magnets at the ceiling and floor (N top, S bottom) both produce a strong axial field in the cavity and, through their dipole field lines, contribute to the guiding of the shell in the polar regions.

The main element of the revision is the 50 cm REBCO superconducting guide/storage coil layer fitted on the outer surface of the inner capsule (Figure 4). The layer produces a 5 T field tangent to the surface along the meridians; combined at the poles with the field of the 10 T pole magnets it forms a magnetic-mirror geometry: 5 T at the equator, 10 T at the polar throats. The layer's mass is 1 070 t and its stored magnetic energy 1.8 GJ. The total mass of the inner capsule with the coil layer is 5 270 t.

Energy shell 1: arc, guiding, storage and laser

30 MV is applied between the W-Re cathode (−) just above the upper pole and the W-Re anode (+) below the lower pole; the electrons leaving the cathode are accelerated to $\gamma = 59.7$ at a current of 20 mA (600 kW). In the previous design the electrons crossed the inner capsule from pole to pole in 63–68 ns and stopped in the anode; in the revised design the 5 T tangential field, together with the 10 T field at the polar throats, confines a substantial fraction of the electrons by reflecting them back and forth along the field lines. The Larmor radius of a 30 MeV electron is 2.0 cm at 5 T and 1.0 cm at 10 T; the shell wraps the inner-capsule surface as a layer about 4 cm thick. The mechanism that sets the confinement time is synchrotron radiation: a $\gamma = 60$ electron gyrating at ~10° pitch angle in 5 T radiates 4.3×10^{-11} W and loses its energy in 0.11 s; larger pitch angles speed up the cooling (as $\sin^2\theta$), smaller ones increase the escape through the mirror. The steady-state stored energy is the product of the injected power and the confinement time: $E_{st} = P_{arc} \times \tau = 1.2$ MW × 0.11 s ≈ 140 kJ (2.8×10^{16} electrons). This corresponds to only one thousandth of the Brillouin density limit (2×10^{18} m^{-3} at 5 T and $\gamma = 60$); space-charge fields and collective instabilities are not limiting at this density. The shell fills in 0.11 s; the radiated synchrotron power (1.2 MW in steady state, in the infrared/visible) is absorbed in the walls and carried away by the water. The electrons that reach the anode (escaping and cooled ones) are the source of positron production (Results).

The Ø10 cm circular laser tip above the cathode sends a 20 kW continuous-wave (1064 nm) ring beam parallel to and in the same direction as the electron shell; the laser is the optical channel of the chopper experiment. The electrodes rotate at 700 rpm and vibrate at 100 Hz; as in rotating-anode X-ray tubes this spreads the 600 kW beam power over the electrode surface.

SRF photon shell

A niobium cavity wall (a = 7.3 m, b = 6.3 m) wrapping the inner capsule 1 m outside the coil layer, with electrode openings at the poles, is a superconducting RF resonator operating at 1.3 GHz with a quality factor $Q = 10^{10}$. The 20 kJ of electromagnetic energy stored in the resonator is a "photon shell" oscillating at the speed of light and surrounding the inner capsule from every direction; since an ILC-type 9-cell cavity stores ~200 J, 20 kJ is equivalent to a hundred cavities. The heat load at 2 K is $P = \omega U/Q = 16$ kW and requires a cryogenic plant of about 11 MW; since a larger stored energy (0.2 MJ) would push the cryogenic power to 100 MW, 20 kJ is taken as close to the engineering upper limit. In the chopper cycles the resonator, whose natural decay time ($Q/\omega = 1.2$ s) is longer than the cut, is emptied within the 1 s cut by an active dump coupler and refilled afterwards.

Energy shell 2: the extra gap

Raising the inner diameter of the extra capsule to 28 m leaves 3.1 m between the outer surface of the outer sphere (r = 10.9 m) and the inner surface of the extra sphere (r = 14 m); the 50 cm W-Re tips fit, and 30 MV corresponds to 9.7 MV/m (below the field-emission threshold for clean electrodes in vacuum). The second shell in the extra gap runs at 30 MV / 20 mA (600 kW); the electrons cross the 39 m half-circumference along the outer-sphere surface in 130 ns. There is no storage in this shell (the only guide field is the rings' 1 T vertical field); its contribution is limited to the in-flight energy and is given separately in Table 3. Its anode is a second positron converter.

Toroidal rings and the rotating platform

The 20 T REBCO toroidal ring fixed to the base platform (inner opening 25 m) centres the extra capsule and rotates clockwise with the platform at 120 rpm; the identical ceiling ring is fixed 2 m above the top of the extra capsule. The top face of the base ring is S and that of the ceiling ring N; the fields add in the same (downward) direction at the capsule centre and give 0.98 T. 20 T is the REBCO field level demonstrated by MIT–CFS [9]; the ampere-turns per ring are 50 MA and the stored energy 10.2 GJ. Lowering the platform to 120 rpm is an engineering necessity: the rim speed of the 33.8 m extra capsule becomes 212 m/s, the centrifugal acceleration 272 g, the hoop stress 122 MPa for SiC-SiC and 541 MPa for tungsten–steel; with a CFRP band this is within the safe range. The metric contribution of the rotation (gravitomagnetic and kinetic-energy terms) is given in Supplementary Note S3; the difference between 700 rpm and 120 rpm in these terms is a factor of 34, and both values are unmeasurable.

Chopper subsystem

The chopper cuts the energy shell for $\tau_c = 1$ s every $T_c = 300$ s (Figure 5a). The laser channel is cut by a Pockels cell + polariser (1 ns edge), the arc channel by a cathode grid modulator (1 μs edge), and the SRF channel by an active dump coupler; the three channels are synchronized by a common timer. The reason for lengthening the cut to 1 s is storage: the electron shell with its 0.11 s confinement time and the SRF shell with its 1.2 s decay time do not empty in a 1 ms cut; a 1 s cut empties the stored shell to 99.98% and brings the modulation depth close to unity. The duty loss is $\tau_c/T_c = 3.3\times10^{-3}$, with 288 cycles and 576 switchings per day. The quantum-field-theory result for the cut (the truncated photon, [3]) is given in Results.

Cameras and positron line

Four precision cameras facing four directions between the two capsules and one camera in the cavity record continuously. The positron line has three stages (Figure 4): (1) the anodes are thick W-Re converters optimized for 30 MeV electrons (bremsstrahlung + Bethe–Heitler); (2) the solid-neon moderator layer behind the converters turns ~1% of the MeV fast positrons into slow positrons of a few eV; (3) the slow positrons are accumulated in the multicell Surko (Penning–Malmberg) trap layer [10, 11] lining the inner face of the outer sphere and transferred to CERN. The inner faces of the outer and extra spheres are lined almost completely with the trap layer as in the author's design; the moderator stage is the link that was missing in the previous version and that determines the number of trappable positrons.

Calculation methods

All numbers in this article are produced by the calculation script calc_v2.py (Supplementary Data), which evaluates the stated (v1) and revised (v2) designs side by side; the full derivations and the complete tables are given in Supplementary Notes S1–S6. Constants are CODATA 2018 values: $c = 2.998\times10^{8}$ m s^{-1}, $G = 6.674\times10^{-11}$ m^3 kg^{-1} s^{-2}, $\hbar = 1.055\times10^{-34}$ J s, $m_e c^2 = 0.511$ MeV, $e = 1.602\times10^{-19}$ C, $\mu_0 = 4\pi\times10^{-7}$ H m^{-1}, $\sigma_T = 6.65\times10^{-29}$ m^2.

Electron kinematics and storage

An electron that traverses 30 MV has $\gamma = 1 + eV/m_e c^2 = 59.71$, $\beta = 0.999860$ and $p = \gamma\beta m_e c = 30.5$ MeV/c. A current of 20 mA is 1.25×10^{17} electrons per second; the transit energies in flight are 41 mJ (shell 1, 20.5 m meridian, 68 ns), 78 mJ (shell 2, 39 m, 130 ns) and 1.4 mJ (laser). The synchrotron power of a $\gamma = 59.7$ electron with pitch angle $\theta = 10°$ in the 5 T guide field is $P_{sync} = 2\sigma_T c U_B \gamma^2 \sin^2\theta = 4.3\times10^{-11}$ W ($U_B = B^2/2\mu_0 = 9.95\times10^{6}$ J m^{-3}), which consumes the electron's 4.9×10^{-12} J in $\tau = 0.11$ s; the steady-state stored energy is $E_{st} = P_{arc}\,\tau = 1.2$ MW × 0.11 s = 140 kJ, $N_{st} = 2.8\times10^{16}$

electrons, density 2×10^{15} m^{-3} in the 14.3 m^3 layer, one thousandth of the Brillouin limit $n_B = \varepsilon_0 B^2/2\gamma m_e = 2\times10^{18}$ m^{-3} [7]. The Larmor radius is 2.0 cm at 5 T and 1.0 cm at 10 T. The SRF heat load is $P = \omega U/Q = 16$ kW at 2 K and the natural decay time $Q/\omega = 1.2$ s [8].

Metric potential budget

Each source contributes $\Phi/c^2 = -G\, M_{eff}/(c^2 r)$ at the cavity centre in the linearized weak-field limit, with $M_{eff} = M$ for rest mass, E/c^2 for magnetic and electrostatic field energy and $2E/c^2$ for energy moving at the speed of light or stored as relativistic kinetic energy (trace of the spatial stress adds a second term equal to the first); r is the mass-weighted effective distance of each source (Table 2). The wall masses are computed from the stated wall thicknesses and densities (SiC-SiC 2.7, tungsten–steel 12.0, lead 11.3, water 1.0 t m^{-3}, REBCO layer 6.0 t m^{-3}). The curvature scale is $K = 8\pi G\, u/c^4$ for an energy density u. The accumulated-heat term uses the full 24-hour energy input (1.22 MW × 86 400 s = 105 GJ) at an effective radius of 9 m as an upper bound; it is removed by the cooling water. The frame-dragging rate of the rotating structure is $\Omega_{LT} \approx 4G\, M\, \omega/(3c^2 R)$ and the quadrupole radiation of each time-dependent process is $L_{GW} = (G/5c^5)\langle(d^3Q/dt^3)^2\rangle$ with the changing quadrupole moment of Supplementary Table S3.

Chopper and truncated-photon analysis

The photons created from the vacuum at a switching edge of duration T are bounded by $\langle n\rangle \le \kappa_0/4T + \kappa_0^2/16T^2$ per one-dimensional channel [3], with κ_0 the time scale that sets the mirror reflectivity ($\kappa_0 = 2\cdot100/\omega_0 = 1.13\times10^{-13}$ s for a transmission of 10^{-4} at 1064 nm); the transverse mode count of the Ø10 cm beam is $A/\lambda^2 = 6.9\times10^9$, and $N_{DCE} = \langle n\rangle\, A/\lambda^2$. The extra energy $N_{DCE}\,\hbar\omega$ is confined to a transition region of width cT; its curvature is $8\pi G\, u/c^4$ with $u = E_{DCE}/(A\, cT)$, and its contribution to the cavity potential $2G\, E_{DCE}/(c^4 r)$. For the electron field the pair-creation time scale is $\hbar/2m_e c^2$. The emptying and refilling of the stored shell follow $\exp(-t/\tau)$ with $\tau = 0.11$ s; the residual after a 1 s cut is 1.6×10^{-4}. The quantum-inequality bound on negative energy density in the transition layer is taken as $u_{min} \approx \hbar c/(cT)^4$ (order of magnitude) [24]. The lock-in exclusion bound is $\xi_{excl} = \sigma_y/|\Phi_s/c^2|$ with σ_y the clock pair's fractional stability after $N_{cycles} = 288$ cycles ($\sigma_y \approx 10^{-18}/\sqrt{N_{cycles}} \approx 5\times10^{-19}$ for an optical lattice clock).

Positron production

The electron number delivered to the anodes in 24 h is $N_e = 2\,(I/e)\,t = 2.16\times10^{22}$. The fast-positron yield of a thick high-Z converter at 30 MeV is taken between 1.5×10^{-2} (conservative) and 3.0×10^{-2} (optimistic) positrons per electron, interpolated from measured and simulated thick-target yields at 25–35 MeV [13, 14]; moderation efficiency of solid neon 10^{-2} and trap retention 0.2 follow the Surko-trap literature [10, 11]. The chopper duty loss is $\tau_c/T_c = 3.3\times10^{-3}$; the burst at each cut is N_{st} × yield. The reference value of 62.5 trillion dollars per gram is used only to express the produced mass in a commonly quoted unit; there is no market.

Power and cost

Continuous power: arcs 1.2 MW, laser 67 kW, cryogenic plant of the 20 T rings ~4 MW, coil layer ~1 MW, pole magnets 0.4 MW, SRF cryogenics ~11.4 MW, platform drive 0.3 MW, anode cooling/vacuum/control 1.5 MW, moderator and trap line 0.3 MW; total 20.2 MW, 485 MWh per 24-hour session, plus 187 MWh to spin the platform up to 120 rpm. Energy is priced at 0.10 $/kWh; other operating costs at 0.5 million dollars per session; capital cost 3–15 billion dollars amortized over 20 years × 100 sessions; the session balance with a 5 million dollar experiment fee is given in Supplementary Table S6.

Measurement protocol and statistics

The magnets, arcs, SRF resonator and laser are energized together; the arcs are raised stepwise from 50–200 μA to 20 mA; the storage shell fills in 0.1 s and the SRF shell in 1.2 s; the system runs for 24 hours. Three clock channels are used: a magnetically insensitive optical clock or a chip-scale atomic clock in the cavity (mu-metal and superconducting shielding are mandatory because of the 10 T pole field), a clock in the cavern outside the shell, and a clock on the rim of the rotating platform that calibrates the chain against a known kinematic value (212 m/s: $v^2/2c^2 = 2.5\times10^{-13}$, 21.6 ns per day). The ON/OFF comparison is made by lock-in at the chopper frequency (3.33 mHz, 288 cycles per session); the chopper period is scanned over 300 s, 60 s and 10 s in three sub-sessions to test a frequency-dependent coupling; the positron bursts at each cut are recorded as the per-cycle measure of the stored shell energy. Blind analysis, multi-clock comparison, cameras-on/off control sub-sessions and independent replication are part of the protocol. The pre-experiment uses a 1 kV, 1 mA electron layer stored in a 0.5 T permanent-magnet mirror around a chip-scale atomic clock, chopped at 1 Hz, with the same two-channel lock-in; its shell term is $\sim10^{-42}$ and it bounds ξ at the 10^{30} level.

Ethics statement

No experiments on humans or animals were performed for this article; it is a theoretical and pre-experimental study. Any future session with a live animal will require prior approval by an institutional animal ethics committee, and the protocol specifies a mannequin with clocks as the first test subject.

Use of artificial intelligence

Artificial-intelligence tools were used for the literature search, for checking and executing the calculations, and for the page layout; the conception, physics, design and interpretation are the author's own, and the author takes full responsibility for the content.

References

1. Börekci, H. Beyond Einstein frame-dragging hypothesis (BEFH): a dual-capsule apparatus to test spacetime isolation. Preprint at Research Square https://doi.org/10.21203/rs.3.rs-9999735/v1 (2026).
2. Börekci, H. Engineering a transient spacetime perturbation with a near-light-speed enclosing energy shell. Preprint at Zenodo https://zenodo.org/records/21828468 (2026).
3. Rukan, I. C. O., Gulla, J. & Skaar, J. Truncated photon. Phys. Rev. Lett. 137, 033601 (2026).
4. Moore, G. T. Quantum theory of the electromagnetic field in a variable-length one-dimensional cavity. J. Math. Phys. 11, 2679–2691 (1970).
5. Wilson, C. M. et al. Observation of the dynamical Casimir effect in a superconducting circuit. Nature 479, 376–379 (2011).
6. Hugenschmidt, C. et al. The NEPOMUC upgrade and advanced positron beam experiments. New J. Phys. 14, 055027 (2012).
7. Davidson, R. C. Physics of Nonneutral Plasmas (Imperial College Press, London, 2001).
8. Adolphsen, C. et al. The International Linear Collider Technical Design Report – Volume 3.II: Accelerator Baseline Design. Preprint at arXiv https://arxiv.org/abs/1306.6328 (2013).
9. Hartwig, Z. S. et al. The SPARC toroidal field model coil program. IEEE Trans. Appl. Supercond. 34, 0600316 (2024).
10. Surko, C. M. & Greaves, R. G. Emerging science and technology of antimatter plasmas and trap-based beams. Phys. Plasmas 11, 2333–2348 (2004).
11. Danielson, J. R., Dubin, D. H. E., Greaves, R. G. & Surko, C. M. Plasma and trap-based techniques for science with positrons. Rev. Mod. Phys. 87, 247–306 (2015).
12. Bothwell, T. et al. Resolving the gravitational redshift across a millimetre-scale atomic sample. Nature 602, 420–424 (2022).

13. Sarri, G. et al. Table-top laser-based source of femtosecond, collimated, ultrarelativistic positron beams. Phys. Rev. Lett. 110, 255002 (2013).
14. Noh, Y. K. et al. GeV-scale charge-neutral pair beams from bremsstrahlung gamma rays. Commun. Phys. 7, 39 (2024).
15. Birkhoff, G. D. Relativity and Modern Physics (Harvard Univ. Press, Cambridge, MA, 1923).
16. Israel, W. Singular hypersurfaces and thin shells in general relativity. Nuovo Cim. B 44, 1–14 (1966).
17. Tolman, R. C., Ehrenfest, P. & Podolsky, B. On the gravitational field produced by light. Phys. Rev. 37, 602–615 (1931).
18. Aichelburg, P. C. & Sexl, R. U. On the gravitational field of a massless particle. Gen. Relativ. Gravit. 2, 303–312 (1971).
19. Bonnor, W. B. The gravitational field of light. Commun. Math. Phys. 13, 163–174 (1969).
20. Rätzel, D., Wilkens, M. & Menzel, R. Gravitational properties of light—the gravitational field of a laser pulse. New J. Phys. 18, 023009 (2016).
21. Spengler, F., Rätzel, D. & Braun, D. Perspectives of measuring gravitational effects of laser light and particle beams. New J. Phys. 24, 053021 (2022).
22. Everitt, C. W. F. et al. Gravity Probe B: final results of a space experiment to test general relativity. Phys. Rev. Lett. 106, 221101 (2011).
23. Lemeshko, A. Gravity and time: a temporal-response framework (lapse N, temporal potential Ψ_T, response coefficient X_T). Unpublished preprint, Kyiv (2026).
24. Ford, L. H. & Roman, T. A. Averaged energy conditions and quantum inequalities. Phys. Rev. D 51, 4277–4286 (1995).
25. Westphal, T., Hepach, H., Pfaff, J. & Aspelmeyer, M. Measurement of gravitational coupling between millimetre-sized masses. Nature 591, 225–228 (2021).
26. Fuchs, T. M. et al. Measuring gravity with milligram levitated masses. Sci. Adv. 10, eadk2949 (2024).
27. Muñoz de Nova, J. R., Golubkov, K., Kolobov, V. I. & Steinhauer, J. Observation of thermal Hawking radiation and its temperature in an analogue black hole. Nature 569, 688–691 (2019).
28. Belgiorno, F. et al. Hawking radiation from ultrashort laser pulse filaments. Phys. Rev. Lett. 105, 203901 (2010).
29. Procopio, L. M., Agüero-Santacruz, R., Bermudez, D. & Leonhardt, U. Backreaction of stimulated Hawking radiation in an optical analogue. Nature (2026, in press).
30. Arrowsmith, C. D. et al. Laboratory realization of relativistic pair-plasma beams. Nat. Commun. 15, 5029 (2024).
31. Aiello, S. et al. (KM3NeT Collaboration). Observation of an ultra-high-energy cosmic neutrino with KM3NeT. Nature 638, 376–382 (2025).
32. Touboul, P. et al. MICROSCOPE mission: final results of the test of the equivalence principle. Phys. Rev. Lett. 129, 121102 (2022).
33. Abbott, R. et al. Tests of general relativity with binary black holes from the second LIGO–Virgo gravitational-wave transient catalog. Phys. Rev. D 103, 122002 (2021).
34. Podkletnov, E. & Nieminen, R. A possibility of gravitational force shielding by bulk $YBa_2Cu_3O_{7-x}$ superconductor. Physica C 203, 441–444 (1992).
35. Le Floch, B. & LeFloch, P. G. Optimal shielding for Einstein gravity. Preprint at arXiv https://arxiv.org/abs/2402.17598 (2024).

Funding

The author received no specific grant or financial support for this research from any funding agency in the public, commercial, or not-for-profit sectors. The work was carried out entirely with the author's own means.

Acknowledgements

The author received no institutional support for the design or writing of this article or of the apparatus and is not employed by any state-affiliated institution; the work was carried out entirely with the author's own means.

Author contributions

H.B. conceived the study, designed the apparatus, defined the three-layer framework, performed and checked the calculations, prepared the figures and wrote the manuscript.

Competing interests

The author declares the following competing interest: a patent application for the "Börekci Energy Field — spacetime dilation and antimatter production system" (TÜRKPATENT application no. 2026/011037, 4 July 2026) has been filed by the author. The author declares no other competing interests.

Data availability

All numerical results in this article are generated by the calculation script calc_v2.py (Python 3) and its output file results_v2.json, which are provided as Supplementary Data with the article; no other datasets were generated or analysed.

Figure legends

Figure 1. Three-dimensional isometric cutaway of the revised triple-capsule apparatus (BEF-2026-R). One quarter of the structure is removed; the drawing is to scale (outermost sphere 33.8 m). Numbered components (key on the right): 1 extra outer capsule (28 m inner diameter); 2 outer capsule (16 m); 3 inner capsule (12 m × 10 m prolate ellipsoid) with its four-layer wall; 4 5 T REBCO guide/storage coil layer; 5 stored relativistic electron shell ($\tau \approx 0.1$ s, ≈140 kJ); 6 SRF photon shell (1.3 GHz, 20 kJ); 7 10 T pole magnets; 8 tungsten–rhenium cathode and anode (arc 1, 30 MV / 20 mA); 9 laser ring tip with Pockels chopper; 10 arc 2 in the 3.1 m extra gap; 11 20 T toroidal rings; 12 rotating base platform (120 rpm); 13 cameras; 14 positron transfer line. Red and orange meridians are the electron and laser shells.

Figure 2. Side view of BEF-2026-R, vertical section through the axis (y > 0 half shown). The stored electron–laser shell (red/orange meridians) wraps the inner capsule from pole to pole between the coil layer (4) and the SRF wall (6); the outer red meridians are the second arc (10) in the extra gap. The ceiling ring (11, fixed) and the base ring on the rotating platform (12) are shown with their 25 m opening. Component numbers as in Figure 1.

Figure 3. Top view of BEF-2026-R, horizontal section in the equatorial plane (upper half removed). The concentric wall layers of the three capsules, the coil layer, the stored shell, the SRF wall, the four cameras (13) in the outer gap, the positron transfer line (14) and the base ring (11) on the platform (12) are visible. Component numbers as in Figure 1.

Figure 4. Detail of the upper pole region (front view). From inside out: the cavity, the water, lead, tungsten–steel and SiC-SiC wall layers of the inner capsule, the 5 T REBCO coil layer, the stored electron layer (red band), the SRF niobium wall and the moderator/trap layer on the inner face of the outer capsule. The 10 T pole magnet at the cavity ceiling and the dipole field lines (dotted) that close the magnetic mirror at the polar throat are shown, together with the tungsten–rhenium electrode (700 rpm, 100 Hz), the laser ring tip, the arc and laser meridians, the Pockels cell and cathode grid of the chopper and their common timer.

Figure 5. Chopper analysis. a, Shell state over 20 minutes: the shell is cut for 1 s every 300 s (288 cycles and 576 switchings per day; duty loss 3.3×10^{-3}); the stored shell empties and refills with $\tau \approx 0.11$ s. **b**, Photons created from the vacuum per switching as a function of the switching time T, per one-

dimensional channel (black) and for the full Ø10 cm beam of 6.9×10^{9} transverse modes (red), from the Rukan–Gulla–Skaar bound $\langle n\rangle \le \kappa_0/4T + \kappa_0^2/16T^2$ with $\kappa_0 = 1.13\times10^{-13}$ s; the points mark a 1 ns Pockels cell (2×10^{5} photons), a 10 ns acousto-optic modulator and a 10 µs mechanical shutter. **c**, Local-equivalence structure of the truncated shell: to the left of the transition region (width $cT = 30$ cm, moving with the light cone) every local measurement gives the statistics of the full shell, to the right those of the vacuum; the $0\ldots\infty$ photon mixture exists only in the global state.

Figure 6. Stated design (v1) versus revised design (BEF-2026-R), logarithmic axes. a, Magnitude of the near-light-speed shell term $|\Phi_s/c^2|$ at the cavity centre. **b**, Coupling parameter ξ excluded by a chip-scale atomic clock, an optical lattice clock, and an optical clock with 3.33 mHz chopper lock-in (288 cycles). **c**, Fast positrons produced and slow positrons trappable per 24-hour session for the conservative (1.5×10^{-2}) and optimistic (3.0×10^{-2}) converter yields. Values from Supplementary Tables S4–S6.

Supplementary Files

This is a list of supplementary files associated with this preprint. Click to download.

- calcv2.py
- resultsv2.json
- BEF2026RSciRepSupplementaryEN.pdf